Modelling Gamma-Ray Spectra of SNRs to predict their Detectability by SWGO

Bachelor's Thesis in Physics

Presented by
Nick Scharrer
October 13, 2022
Erlangen Centre for Astroparticle Physics
Friedrich-Alexander-Universität Erlangen-Nürnberg

Supervisor: Dr. Alison Mitchell

Abstract

Supernova remnants (SNR) are known as cosmic particle accelerators and sources of highly energetic gamma-rays. This makes them an interesting object for astroparticle physics to better understand the mechanisms of particle acceleration in cosmic objects and the origin of cosmic rays. However, to be able to study SNRs and similar objects in more detail new and more powerful detectors are needed. One planned facility is the Southern Wide-field Gamma-ray Observatory (SWGO) which will be sensitive for gamma-rays with energies ranging from 100 GeV up to a few 100s TeV. In this thesis, the gamma-ray spectra produced by proton-proton interaction will be modeled for a set of SNRs to determine which SNRs are bright enough so they could possibly be detected by SWGO and which of these are located in the southern sky and will actually be detectable by SWGO. Also a closer look on some of these SNRs will be taken and the model used to predict their flux will be compared to actual data to estimate the accuracy of the model.

Contents

1 Introduction

After Henri Becquerel discovered radioactivity in 1896, people thought that ionizing radiation is only emitted by rocks and soil. In 1904 Franz Linke published his results from different atmospheric measurements he made using weather balloons [13]. He had found that the ionization first drops but then starts to rise again between 1 and 3 km to finally exceed the value measured at ground level. Unfortunately, regarding to his measurement uncertainties, he still concluded that the origin of the ionisation has to be searched on the ground and not in space. In 1912, though, Victor Hess published his results from similar balloon flights, but he came to a different conclusion which had a greater impact [12]. He recognized that since the radiation first drops with rising altitude, the influence of radiation from the ground must decline. And the dramatic rise of ionization after a few kilometers could therefor not be reasonably described by radioactive atoms in the air. So he eventually came to the conclusion that this can only be described by radiation that enters the earths atmosphere from above. After these discoveries many other experiments were conducted to study this radiation which became known as Cosmic Rays.

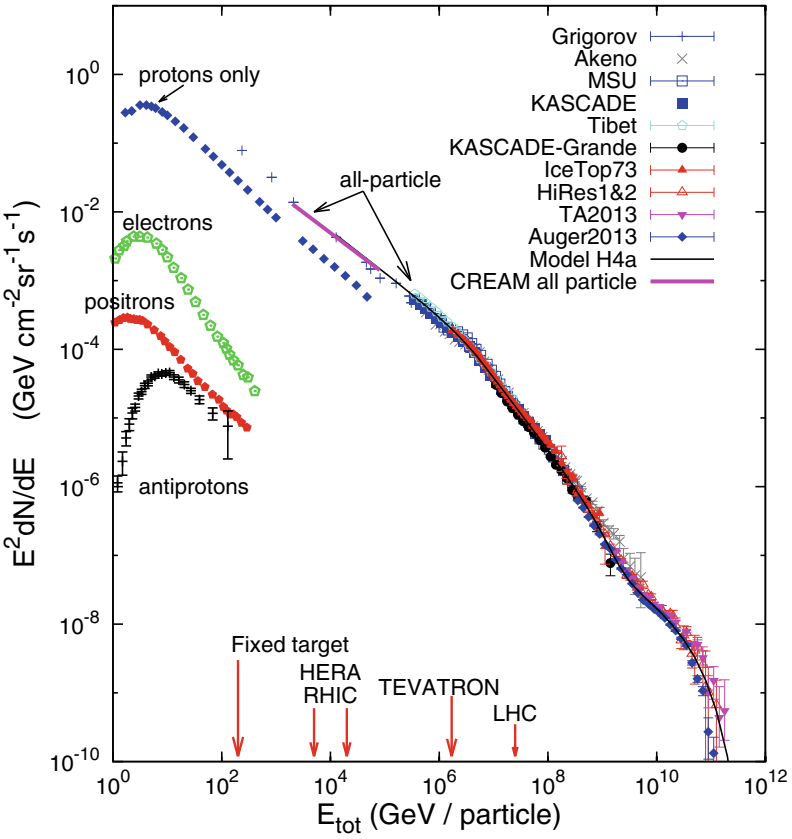

Figure 1: The measured spectrum of Cosmic Rays (Source: [7])

Cosmic rays consist of gamma-rays, electrons, protons and heavier nuclei. Their spectrum is well known today and follows a power-law $\propto E^{-2.7}$ until the so called "knee" at $E \approx 1\,\mathrm{PeV}$, where the slope changes to be $\propto E^{-3.1}$. However, it is still not fully understood where the Cosmic rays exactly originate from, especially for the higher energy regimes beyond the knee. Since they are deflected by magnetic fields, charged particles aren't suitable to determine their sources, but gamma-rays travel through the interstellar medium (ISM) practically undisturbed. So by detecting highly energetic gamma-rays we can tell that their sources can sufficiently accelerate particles that produce them.
One known kind of sources of gamma-rays are Supernova Remnants (SNR), the off-blown shell of a star that has ended in a supernova. There are dozens of known SNRs and a lot of suspected candidates. Because a supernova ejects energy in the order of $E_{51} = 10^{51}\,\mathrm{erg}$, SNRs are very good accelerators and thus are suggested to be PeVatrons, which means they may able to accelerate particles up to the PeV range, but that still has to be proven. The majority of known SNRs is located in the northern sky, which is apparently not due to an non-isotropic distribution of SNRs, but due to the historical fact that most of the astronomical science and observation happened in the northern hemisphere. So to learn more about SNRs and their production of gamma-rays we need to install more powerful detectors also in the southern hemisphere to further investigate SNRs that are located there.
Gamma-rays can either be detected directly via orbiting satellites like Fermi or indirectly via ground-based detectors. Ground-based experiments detect the Cherenkov light that is emitted by secondary particles which are produced by cosmic gamma-rays hitting nuclei in the earths atmosphere, resulting in a extensive air shower [17]. There are two types of ground-based detectors. One method uses telescopes to measure the Cherenkov light in the atmosphere, like HESS in Namibia, the other method uses photomultipliers in water-filled tanks to measure the Cherenkov light like HAWK in Mexico.
One future experiment that will be discussed in more detail is the Southern Wide-field gamma-ray Observatory (SWGO). It is a particle detector that is planned to be build up on a plateau in the mountains of Southern America at an altitude $\geq 4.4\,\mathrm{km}$. Similar to HAWK it will be an array of water-filled tanks that are distributed in circular areas with decreasing density at larger distances from the center, as shown in figure 2. The total area will be roughly $0.3\,\mathrm{km}^2$. It will be the first detector of this kind in the southern hemisphere and will detect gamma-rays from 100 GeV up to a few 100 TeV [5]. Because of its architecture, SWGO has a field of view of 90° and can detect nearly without interruption, since it doesn't need to be adjusted onto a desired spot in the sky and can also collect data during the day. That makes it a perfect detector to survey the southern sky and search for new SNRs.

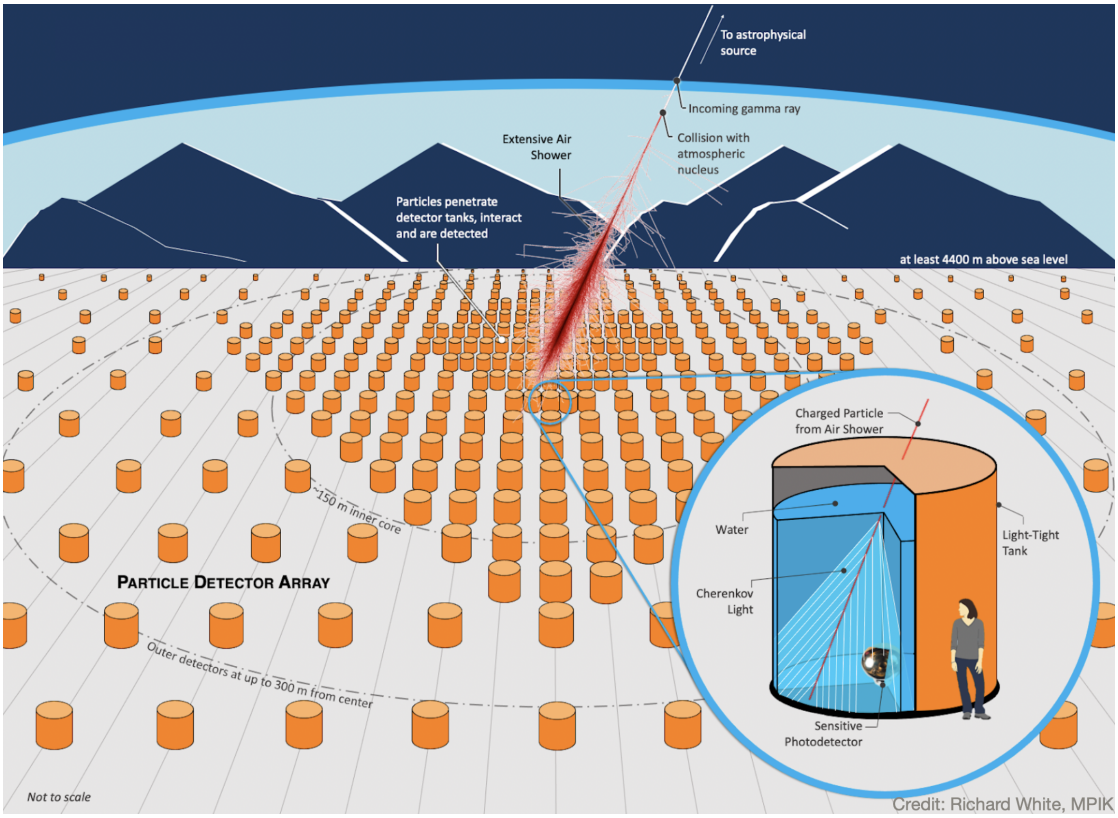

Figure 2: A schematic image of the SWGO detector array (Source: [16])

This thesis' aim is to predict the gamma-ray spectra of a set of known SNRs to investigate which of these could be detectable by SWGO according to its sensitivity and which of them are indeed detectable by SWGO, i.e. are in the southern sky that will be covered by SWGO. To achieve this, a reasonable model is needed to predict the gamma-ray spectra of SNRs an compare them to the spectral range SWGO will be sensitive to.

2 Model

To better understand how SNRs produce gamma-rays, a closer look into the shock mechanism will be taken, how this causes particle acceleration and eventually the production of gamma-rays. After discussing the processes of gamma-ray production a closer look into the evolution of SNRs and describing equations will be taken. And finally a description of the proton spectrum of an SNR will be given.

2.1 Shock Mechanism and Particle Acceleration

When a star turns into a Supernova, it ejects an expanding shell of mass that creates a shock wave propagating at supersonic speed ahead of the ejecta into the ISM. The ISM then accelerates, compresses and heats up. This forward shock follows an inwards shock that, in turn, decelerates, compresses and heats up the ejecta. Within the shock wave expanding into the ISM particles can be accelerated via a process called first order Fermi acceleration [19].
When a particle of the ISM crosses the shock front downstream, it encounters a turbulent magnetic field carried by the outwards moving shocked plasma. There it scatters diffusely at this field and gains energy through this head-on elastic collision. It then crosses the shock upstream entering the ISM again which now moves towards the particle in its frame of reference, hence it gets scattered again at the turbulent magnetic field in the ISM and propagates back towards the shock. So the particle gradually gathers energy in this process.

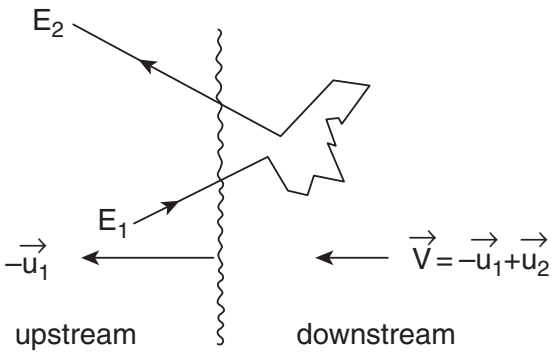

Figure 3: Scheme of the shock front moving with $-\vec{u}_1$ into the ISM, the shocked matter then has a smaller velocity $\vec{u}_2$ with respect to the shock, so the gas behind the shock moves with $\vec{V}$ in the lab frame. Thus, from the particles frame of reference the gas on both sides flows towards the shock (Source: [19]).

Due to the random scattering it is an statistical progress where the probability of escaping rises with the particles energy. The maximum Energy a particle can reach is limited by the Hillas criterion, which takes the fact into account, that an accelerator of size L can

only hold particles in its magnetic field that have a gyroradius $r_g < L$ [6]:

$$E_{\max} = eZBL\beta c. \tag{1}$$

Where e is the elementary charge, Z is the charge number of the particle, B is the magnetic field and the particles speed given as βc with $\beta \simeq 1$. About 10 % of the energy ejected by a SNR is consumed in this acceleration process.

2.2 Gamma-Ray Production

For the particles accelerated in the SNR there are four relevant processes of gamma-ray production:

1. Bremsstrahlung:
   When a charged particle gets deflected and thereby accelerated in the Coulomb field of another charged particle, it emits Bremsstrahlung. Since the cross section $\sigma_B = \frac{e^4}{m^2}$ declines with bigger masses, the spectrum of Bremsstrahlung is dominated by electrons. In this interaction the electrons lose the majority of their energy by emitting up to two photons.

2. Synchrotron Radiation:
   As a charged particle gets accelerated along a magnetic field it propagates on a helical trajectory and emits Synchrotron radiation in the directions perpendicular to the magnetic field. This process is also dominated by electrons since they produce Synchrotron radiation of much higher energies than protons.

3. Inverse Compton Scattering:
   In this process, that is also dominated by electrons, a particle of high energy scatters on a low-energy photon and transfers a part of its energy to it resulting in a photon with an energy up to a few 10 TeV. The needed low-energy photons are mostly provided by the cosmic microwave background.

4. Proton-Proton Interaction:
   Highly energetic protons can produce other particles, mostly pions, via inelastic collisions with other protons or hadronic particles in general. Although π^+, π^- and π^0 are produced with equal probability at high energies, only the π^0 decays into two photons that have around 10 % of the protons initial energy each.

Of these four processes, p-p interaction produces the gamma-rays of highest energies and highest flux, so p-p interactions are dominant in the energies relevant for SWGO and so it is sufficient to restrict the analysis in the following on this process.

2.3 SNR Evolution

During its lifetime, a SNR undergoes four different phases that differ in the change of the SNRs' radius over time:

1. free-expansion or ejecta-dominated phase:
   In this phase the SNR expands nearly unimpeded into the ISM at constant speed. Its speed depends on the type of supernova and ranges from $5000\,\mathrm{km\,s^{-1}}$ for core collapse supernovae to $10^4\,\mathrm{km\,s^{-1}}$ for type Ia, which occur in binary systems of white dwarfs and red giants [15]. Since the SNR is freely expanding, its radius is simply described as linear in time, i.e. $R(t) = v \cdot t$. This state of expansion remains until the SNR reaches the Sedov time [6]:

$$t_{\mathrm{Sed}} = 1.6 \cdot 10^3 \left(\frac{E}{E_{51}}\right)^{-\frac{1}{2}} \left(\frac{M_{\mathrm{ej}}}{10 M_\odot}\right)^{\frac{5}{6}} \left(\frac{\rho_0}{10^{-24}\mathrm{g\,cm^{-3}}}\right)^{-\frac{1}{3}} yr. \tag{2}$$

2. Sedov-Taylor or energy-conservation phase:
   The SNR has swept up so much mass from the interstellar medium that this now exceeds the initially ejected mass. However, the energy of the SNR is still conserved in thermal and kinetic energy. Due to the increasing mass, the velocity declines and the radius is then described by the Sedov-Taylor equation [20]:

$$R(t) = \left(\xi_0 \frac{E_{\mathrm{ej}}}{\rho_0}\right)^{\frac{1}{5}} t^{\frac{2}{5}} \tag{3}$$

   Where $\xi_0 = 2.026$ is a constant factor, the ejected energy E_{ej} of the SNR is in units of E_{51}, the age t is given in s and $\rho_0 = 10^{-24}\,\mathrm{g\,cm^{-3}}$ is the density of the ambient ISM.

3. snow-plough or pressure-driven phase:
   Now the energy isn't longer conserved since radiative losses aren't longer negligible, that's why it's also called the radiative phase. In this phase, however, the momentum is conserved and the radius' dependency on time goes down to $R(t) \propto t^{\frac{1}{4}}$. The age at which the SNR transfers into this stage of its evolution is described by [21]:

$$t_{\mathrm{rad}} = 1.4 \cdot 10^{12} \left(\frac{E_{51}}{\rho_0}\right)^{\frac{1}{3}} s \approx 44600 \left(\frac{E_{51}}{\rho_0}\right)^{\frac{1}{3}} yr \tag{4}$$

   Which are ≈96000 yr for typical values.

4. merging phase:
   After around 10 million years the velocity of the shell has dropped to sound speed and its radius remains practically constant at nearly 100 pc.

The theoretical evolution of the SNRs' radius within the different phases is shown in figure 4.

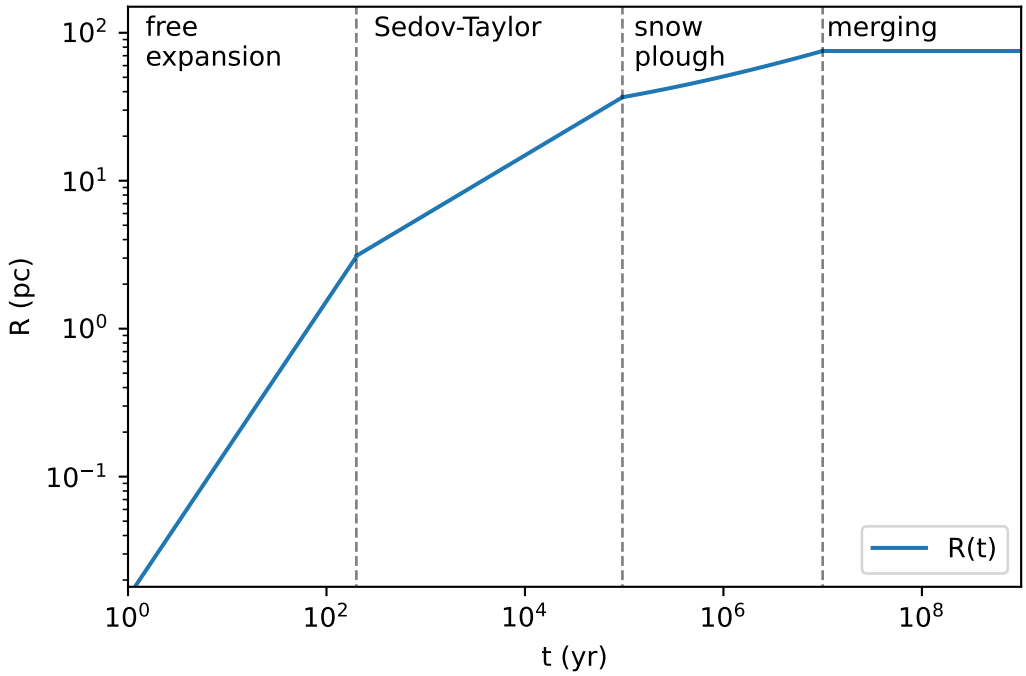

Figure 4: The theoretical evolution of a typical SNRs radius during its lifetime separated into the four phases of expansion

2.4 Proton Spectrum

To be able to calculate a gamma-ray spectrum for a given SNR, a proton energy spectrum is needed first. The energy spectrum of protons in an SNR can be described by a power-law with a cutoff at a highest energy $E_{0,\mathrm{p}}$ [7]:

$$J_\mathrm{p} \equiv \frac{dN_\mathrm{p}}{dE_\mathrm{p} dV} = K_\mathrm{p} E_\mathrm{p}^{-\alpha_\mathrm{p}} \exp\left(-\left(\frac{E_\mathrm{p}}{E_{0,\mathrm{p}}}\right)^{-\beta_\mathrm{p}}\right). \tag{5}$$

The values of the exponents are typically chosen to be $\alpha_\mathrm{p} = 2$ and $\beta_\mathrm{p} = 1$, K_p is a normalization factor given by:

$$w_\mathrm{p} = \int_{100\,\mathrm{GeV}}^{\infty} E_\mathrm{p} J_\mathrm{p}(E_\mathrm{p}) dE_\mathrm{p} = 1\,\mathrm{erg\,cm^{-3}}. \tag{6}$$

. Substituting equation 5 gives an expression for K_p:

$$K_\mathrm{p} = \frac{1\,\mathrm{erg\,cm^{-3}}}{\int_{100\,\mathrm{GeV}}^{\infty} E_\mathrm{p}^{1-\alpha_\mathrm{p}} \exp\left(-\left(\frac{E_\mathrm{p}}{E_{0,\mathrm{p}}}\right)^{-\beta_\mathrm{p}}\right) dE_\mathrm{p}}. \tag{7}$$

The maximum possible energy $E_{0,\mathrm{p}}$ in equation 5 is confined by the Hillas criterion and by the fact, that in the transition between free-expansion phase and Sedov-Taylor phase the shock decelerates and thus the most energetic particles are able to propagate upstream [19]. So the highest energy is reached at t_{Sed} and the maximum energy for particles escaping at $t > t_{\mathrm{Sed}}$ is described by [6]:

$$p_{\mathrm{max},0}(t) = p_{\mathrm{M}} \left(\frac{t}{t_{\mathrm{Sed}}} \right)^{-\delta} \equiv E_{0,\mathrm{p}}. \tag{8}$$

Where p_{M} is the maximal possible energy at $t = t_{\mathrm{Sed}}$ and the value of δ is usually between 1 and 4, so the average of 2.5 is often chosen. p_{M} can be calculated using equation 1. This also requires the size L of the region of acceleration at t_{Sed}, which can be obtained via the fraction:

$$\begin{aligned} \frac{R(t_{\mathrm{Sed}})}{R(t)} &= \left(\frac{t_{\mathrm{Sed}}}{t} \right)^{\frac{2}{5}} \\ \Leftrightarrow R(t_{\mathrm{Sed}}) &= R(t) \left(\frac{t_{\mathrm{Sed}}}{t} \right)^{\frac{2}{5}}. \end{aligned} \tag{9}$$

This gives the radius at t_{Sed} depending on the actual size and age of the SNR and on its Sedov time. This ultimately gives $p_{\mathrm{max},0} \propto t_{\mathrm{Sed}}^{\delta+0.4}$ via equations 1 and 9. Note that equation 3 describes the radius in the Sedov-Taylor phase, thus the evaluation at t_{Sed} is an approximation since t_{Sed} is the transition point between free-expansion and Sedov-Taylor phase.
So by a given radius and age of an SNR, the ejected energy can be calculated via equation 3 and with that the Sedov time and ultimately $p_{\mathrm{max},0}$. Inserting this into equation 5 gives the current distribution of protons. However, equation 5 gives a quantity per unit volume, so it still has to be integrated over the SNRs volume which is a shell that is an estimated 10 % of its radius thick. After renormalisation of the particle spectrum considering that the particles in sum take about 10 % of the ejected energy, the resulting power law can be converted into a spectral energy distribution (SED) of gamma-rays.

3 Results

In this section, gamma-ray spectra for a set of SNRs will be calculated under different conditions to see which ones have a high enough flux to be possibly detected by SWGO and which one of these it actually will detect.

3.1 Selecting a Set of Sources from SNRcat

To get a set of SNRs and their physical properties SNRcat was used. SNRcat is an online catalogue containing 383 entries of known or possible SNRs and information like the age, distance and angular size of them. So first, all of the uncertain entries must be excluded to ensure only actual known SNRs remain. Then those entries where some information about the physical properties is missing are also excluded. And since the most energetic particles are produced at t_{Sed}, SNRs that are much younger can be excluded as well as SNRs older than t_{Rad}, i.e. only SNRs with an age between 300 yr and 96000 yr are chosen. Finally, as the ejected energy is assumed to be around E_{51}, the ejected energy will be restricted to be between $0.1 \cdot E_{51} \leq E_{\mathrm{ej}} \leq 10 \cdot E_{51}$. After applying these criteria a set of 38 SNRs remains.

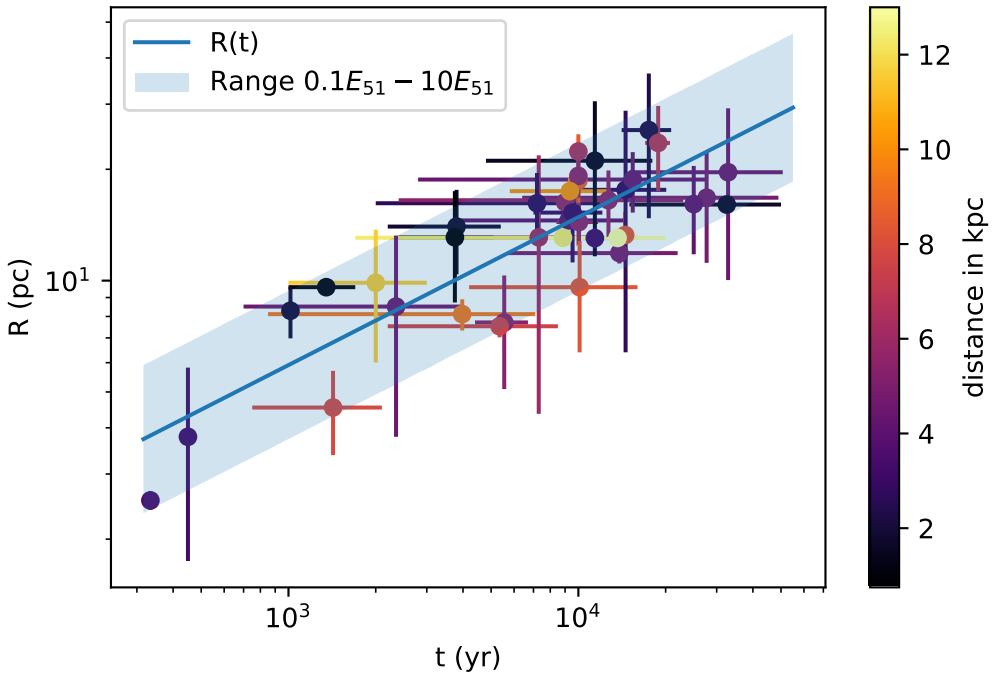

Figure 5: All 38 SNRs together with the theoretical radius from equation 3 and the range for the allowed E_{ej}

3.2 Calculation of Spectra and Flux Predictions

Applying the equations from section 2.4 gives the particle spectra in figure 6. The three candidates that are shifted to higher energies, i.e. have a higher cutoff energy, are described in table 1. It shows that the actual ages are smaller than t_{Sed} which causes that the fraction t/t_{Sed} in equation 8 gets < 1 and thus $p_{\mathrm{max},0} > p_{\mathrm{M}}$. In addition, equation 3 does not hold for an age smaller than the Sedov time. However, this has not much influence on the overall result as it is shown later.

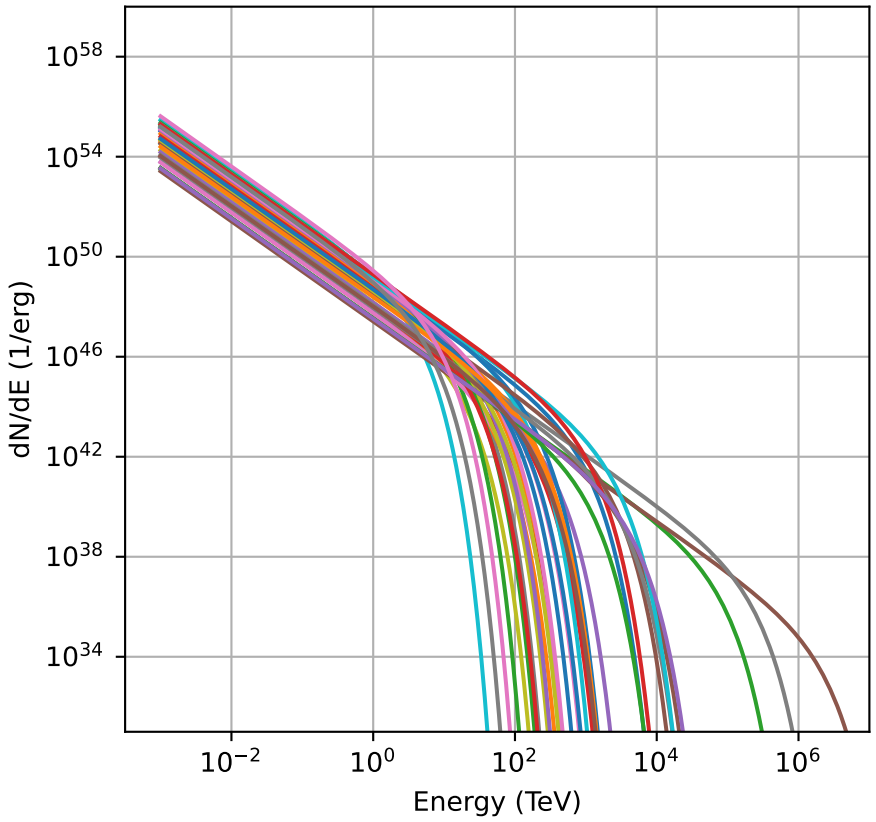

Figure 6: Proton spectra for every SNR calculated at $\delta = 2.5$, $\rho_0 = 1\, m_{\mathrm{p}}\mathrm{cm}^{-3}$, an ejected mass of $M_{\mathrm{ej}} = 10 M_{\odot}$ and an ambient magnetic field of $B = 3\,\mu\mathrm{G}$.

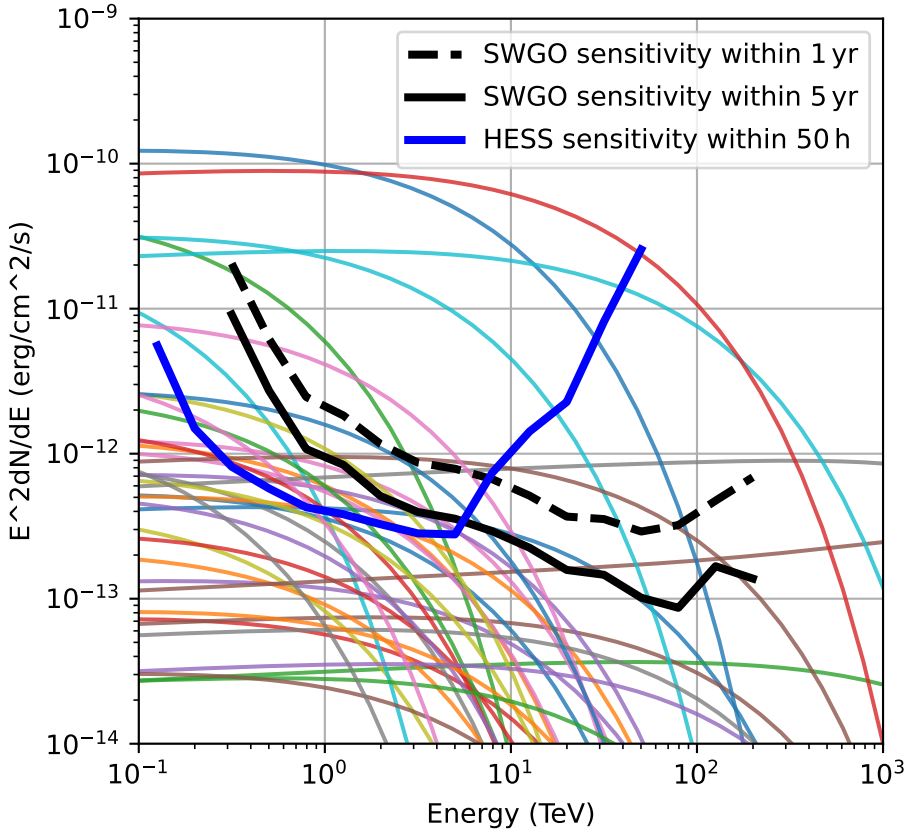

Figure 7: The SEDs calculated from the spectra in figure 6.

Colour	Name	Age (yr)	t_{Sed} (yr)
●	Cas A	$\approx$ 334	$\approx$ 4391
●	Tycho	450	$\approx$ 2199
●	Kes 73	$\approx$ 1425	$\approx$ 4414

Table 1: The three SNRs with the highest cutoff in figure 6 together with their age and the Sedov times used to predict the spectra

The particle spectra can now be passed to GAMERA, which is a library that can process data of particle and gamma-ray sources. It then will calculate the gamma-ray SEDs resulting from the p-p interactions. Which produces the SEDs plotted in figure 7. According to the values used in figure 7 SWGO would be able to detect 8 SNRs after one year and 13 after 5 years respectively. However, of these 13 candidates only 8 are in the southern sky and thus detectable for SWGO as shown in table 2. HESS would be able to detect 8 of these, but only 4 of them have been actually identified. In the case of Puppis A HESS tried to detect it, but has measured less TeV emission than theoretically

expected [11].
The other three sources that were missed by HESS:
G309.2-0.6 has been detected in X-rays and is said to be in the ejecta-dominated phase [14]. That means that the particle acceleration has not yet reached the maximum possible energy and therefor isn't able to emit gamma-rays up to the predicted cutoff, which can be the reason why it is missed by HESS. This agrees with the model since the range of possible ages is 700-4000 yr, but the predicted Sedov time is ≈ 1500 yr.
G332.5-05.6 has been detected in radio, X-rays and gamma-rays [18][2] but the gamma-ray detection by Fermi was only classified to potentially be SNR related.
The predicted SED for G015.9+00.2 is rather low and also crosses the 5 yr sensitivity curve of SWGO only within a few 10 TeV. That means that this source might not be clearly detectable by SWGO too, since not enough data will be collected. In table 2 it also says that Kes 73 has been detected by HESS, but only within a cluster of other sources [4].
The list of all 38 SNRs can be found in table 3. Four of the sources below the dashed line had been detected by HESS although they are predicted to be not detectable. However, these sources where detected by HESS within other sources and identified by their known position, but the model treats them as isolated objects. Another four sources were missed by HESS, although they are predicted to be detectable. However, they only slightly exceed the sensitivity curve and it is therefor predicted that little if any data will be detected.

Source	Name	Detectable after 1 yr	Detectable after 5 yr	Detectable by HESS	Detected by HESS	Location	Flux for $E > 1$ TeV (TeV cm^{-}2 s^{-}1)	Flux for $E > 10$ TeV (TeV cm^{-}2 s^{-}1)
G347.3-00.5	RX J1713.7-3946	Yes	Yes	Yes	Yes	SH	1.67e-10	5.39e-11
G327.6+14.6	SN1006, PKS 1459-41	Yes	Yes	Yes	Yes	SH	6e-11	2.54e-11
G266.2-01.2	Vela Jr, RX J0852.0-4622	Yes	Yes	Yes	Yes	SH	1.04e-10	1.17e-11
G120.1+01.4	Tycho, 3C10, SN1572	Yes	Yes	Yes	No	NH	4.51e-12	3.44e-12
G260.4-03.4	Puppis A, MSH 08-44	Yes	Yes	Yes	(Yes)	SH	2.05e-11	1.6e-12
G309.2-00.6		Yes	Yes	Yes	No	SH	2.19e-12	8.89e-13
G315.4-02.3	RCW 86, MSH 14-63	Yes	Yes	Yes	Yes	SH	2.73e-12	6.95e-14
G089.0+04.7	HB21	Yes	Yes	Yes	No	NH	2.01e-12	8.49e-16
G111.7-02.1	Cassiopeia A (Cas A), W81, 3C461	No	Yes	No	No	NH	1.16e-12	9.51e-13
G015.9+00.2		No	Yes	Yes	No	SH	7.59e-13	2.3e-13
G332.5-05.6		No	Yes	Yes	No	SH	1.2e-12	5.07e-14
G038.7-01.3		No	Yes	Yes	No	NH	6.93e-13	4.21e-14
G166.0+04.3	VRO 42.05.01	No	Yes	Yes	No	NH	5.86e-13	5.96e-15
G027.4+00.0	(Kes 73), 4C-04.71	No	No	No	(Yes)	SH	1.68e-13	1.2e-13

Table 2: List of SNRs that are detectable by SWGO and HESS respectively according to figure 7

3.3 The sky of SNRs seen by SWGO

Another interesting aspect is the distribution of the different SNRs in the sky. Figure 8 shows four different plots of the SNRs' galactic coordinates and their flux. According to the model, SWGO will be able to see the eight SNRs in the lower right plot. So of all 38 considered SNRs only the few ones that are in the southern sky and that have a high flux will be detected. The one SNR that is located nearly 15° above the galactic plane is SN1006. This one together with a few other examples will be highlighted next.

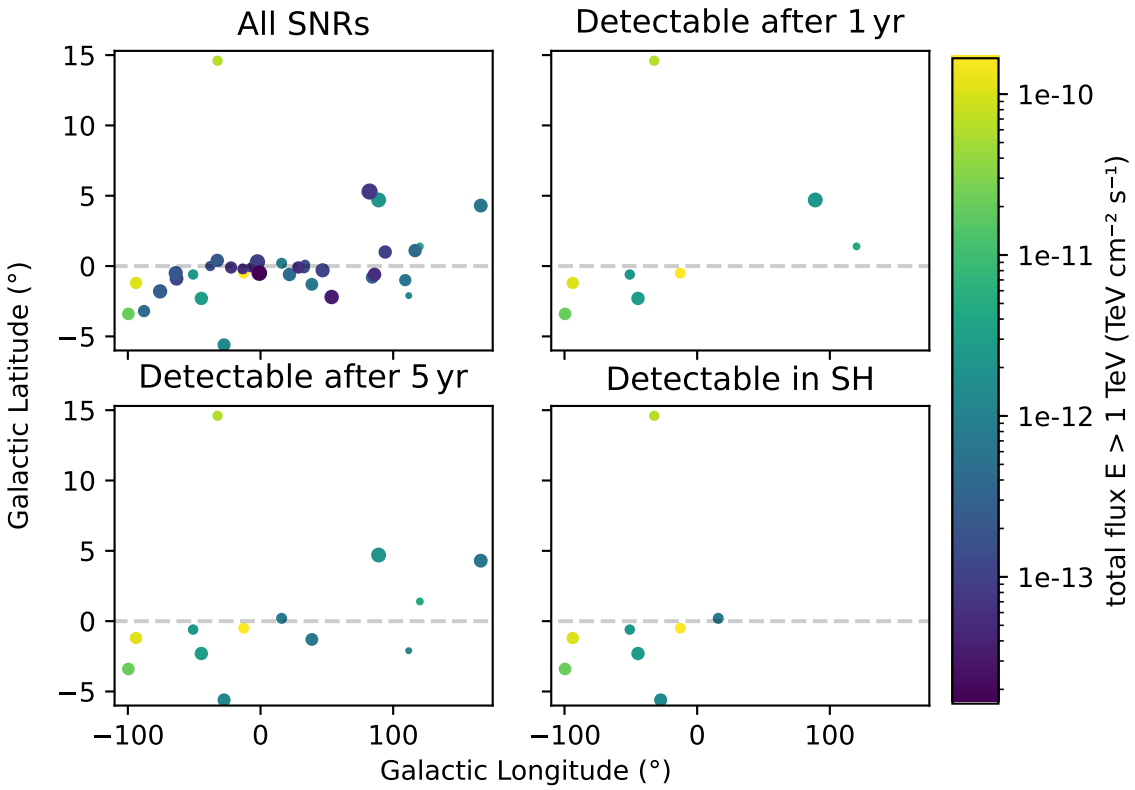

Figure 8: The galactic coordinates of all SNRs and only those predicted to be detectable by SWGO respectively

3.4 Examples of detectable SNRs

RX J1713.7-3946

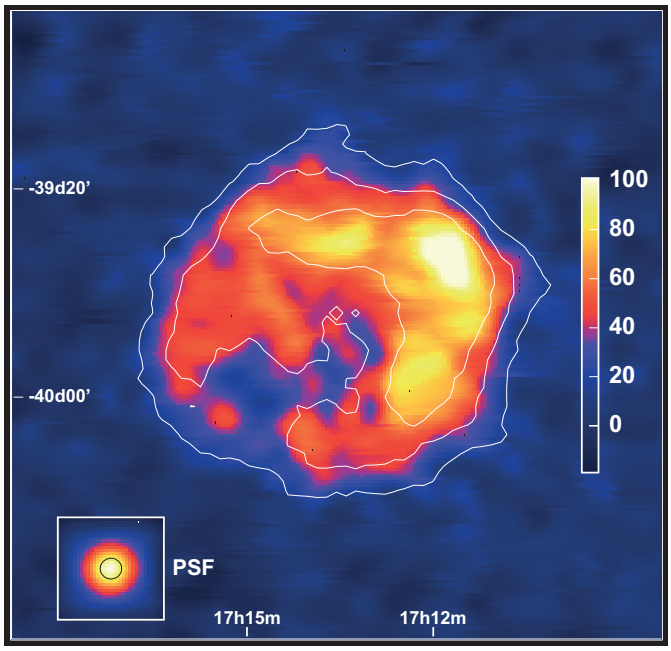

Figure 9: A gamma-ray image of RX J1713.7-3946 from HESS (Source: [3])

RX J1713.7-3946 is the SNR with the highest predicted flux. It has an age of $\approx 1350\,\mathrm{yr}$, a radius of $\approx 9.6\,\mathrm{pc}$ and is located at a distance of $\approx 1.1\,\mathrm{kpc}$. What's special about it is that there are signs that it is surrounded by dust clouds which results in more particles that can be accelerated via shock-cloud interactions and thus in a higher flux [9].

SN1006

SN1006 is 1016 years old, has a radius of $\approx 8.3\,\mathrm{pc}$ and a distance of $\approx 1.9\,\mathrm{kpc}$. As it is shown in figure 10 HESS has only taken data from a north-east and a south-west region of SN1006, which can be explained by SN1006s' magnetic field. Its suggested that it's oriented along these two regions and thus causes the particle acceleration along the shock to be much more efficient there [1]. The model, however, assumes an isotropic magnetic field and thus predicts a flux for the whole size of the SNR. So the modeled SED is significantly higher than the measured data as it is shown later.

Vela Junior

Vela Junior has an age of $\approx 3750\,\mathrm{yr}$, a radius of $\approx 13.1\,\mathrm{pc}$ and a distance of $\approx 0.75\,\mathrm{kpc}$. It overlaps with Vela itself and contains other sources as well, what probably could make it difficult for SWGO to distinguish it from these nearby sources.

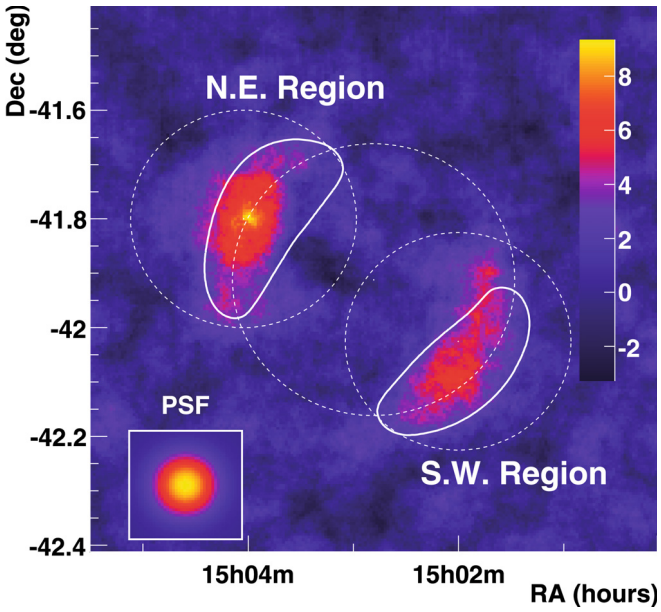

Figure 10: A gamma-ray image of SN1006 taken by HESS (Source: [1])

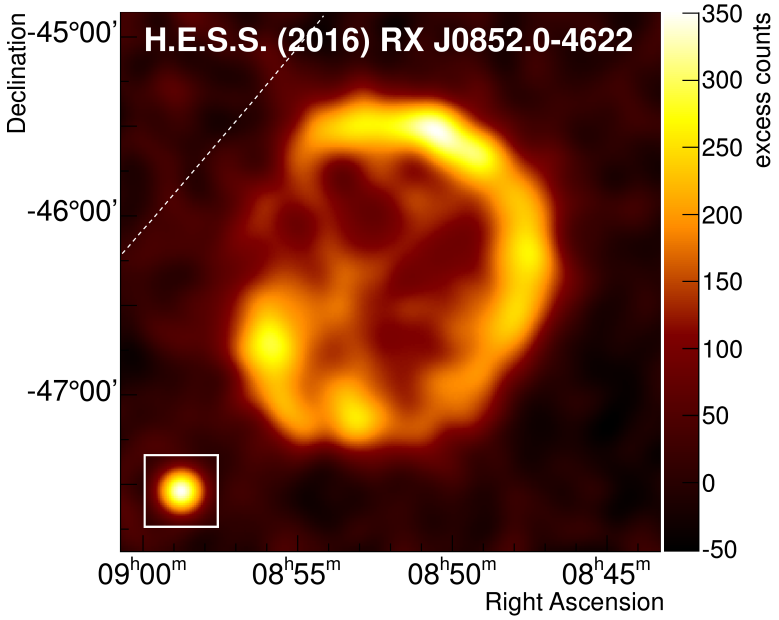

Figure 11: Image of Vela Junior taken by HESS (Source: [10])

Puppis A

Puppis A is $\approx 3800\,\mathrm{yr}$ old, has a radius of $\approx 14\,\mathrm{pc}$ and a distance of $\approx 1.75\,\mathrm{kpc}$. As mentioned above, HESS has measured a lack of TeV emission from Puppis A, although it is a bright source in the X-ray spectrum [8]. But it is also surrounded by molecular clouds that could have suppressed the acceleration of particles and caused a lower cutoff than expected [11], what could explain why the detections don't show the predicted behavior.

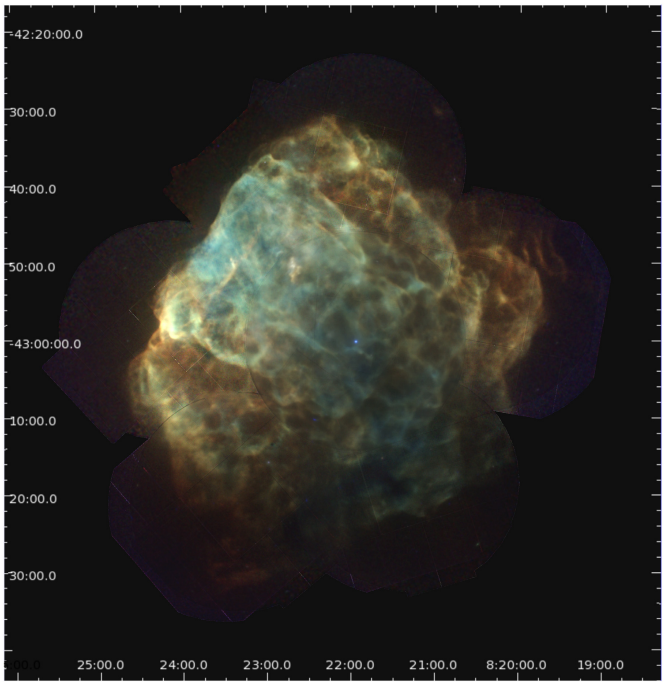

Figure 12: X-ray image of Puppis A obtained from XMM-Newton and Chandra data (Source: [8])

Given these individual features of the SNRs it is a justified question to ask how reasonable the modeled spectra are in comparison to actual data. Because the model assumes for every SNR a uniform expansion into a homogeneous ISM described by equation 3, which is a simplification that not applies generally for all SNRs. However, the model produces spectra that are comparable to the actual data as it is shown in the following.

4 Discussion of the data and Conclusion

To see how well the model is able to predict data, the predicted curves of RX J1713.7-3946, Vela Junior, Tycho and SN1006 will be compared to measured data under various conditions.

4.1 Comparison of the Model with Data under Variation of specific Values

In figure 13 the model is compared using the standard values. The SEDs for RX J1713.7-3946, Vela Junior and Tycho are on the same order of magnitude as the data. The lower plot shows that the data may deviate by a factor of two, but the model is within the error margins for the majority of data points. However, the predicted cutoff for RX J1713.7-3946 is higher than the cutoff in the data. In addition, most of the data of Vela Junior is higher than the model and shows a greater curvature, so it drops faster what indicates a lower cutoff energy. It is also shown that the SED for SN1006 is higher than the data by a factor of about 40. That is because the model predicts an emission from a whole disc, but HESS only measured data for two small regions. So the measured flux is much smaller than the modeled. The reason why also the data of Tycho is compared, although it's not in the southern sky and therefor not detectable, is to show that the model is also able to predict reasonable values for fairly young SNRs.
Now by varying the values of δ, ρ_0, M_{ej} and B the SEDs will shift and come closer to the data under some of the changes. For better visibility, the data of SN1006 is excluded in the following plots, it would change similar to the other curves.
In the shaded area in figure 14 only the value of δ varies. Since δ is the cutoff exponent in equation 8, the cutoff of the SEDs changes a lot. So a smaller δ results in a higher cutoff and vice versa.
The ejected mass of a supernova can vary depending on the original stars mass and the type of supernova. As shown in figure 15 the curves change significant within a range of $10\,M_{\odot}$, because the ejected mass changes the Sedov time and thereby p_{M}. So a lower ejected mass results in a lower cutoff energy.
The effect of a varying density of the surrounding ISM is slightly different. There is the change in Sedov time, because $t_{\mathrm{Sed}} \propto \rho_0^{-1/3}$, which lowers $p_{\mathrm{max},0}$ with rising density. But a higher density also means a higher ejected energy in equation 3 for a given age and radius. In other words, in a denser ISM, the supernova had to eject the same mass with greater energy to leave a SNR of same size. That reduces the cutoff in figure 16, but enlarges the flux at lower energies in parallel.
The cutoff energy also changes under a varying magnetic field. A stronger magnetic field causes a higher maximum energy in the Hillas Criterion as the SNR is able to confine particles of higher energies. The histograms in figure 17 show that E_{max} can vary between a few PeV for $B = 3\,\mu$G and over 100 PeV for $B = 100\,\mu$G.
So in figure 18 the cutoff rises with a stronger field. But $B = 3\,\mu$G seems more reasonable since the cutoffs in the data tend to be lower as the model predicts.
The uncertainties on the given values that are depicted in figure 5 also need to be considered. For example, taken the uncertainty on the SNRs age into account varies the ejected

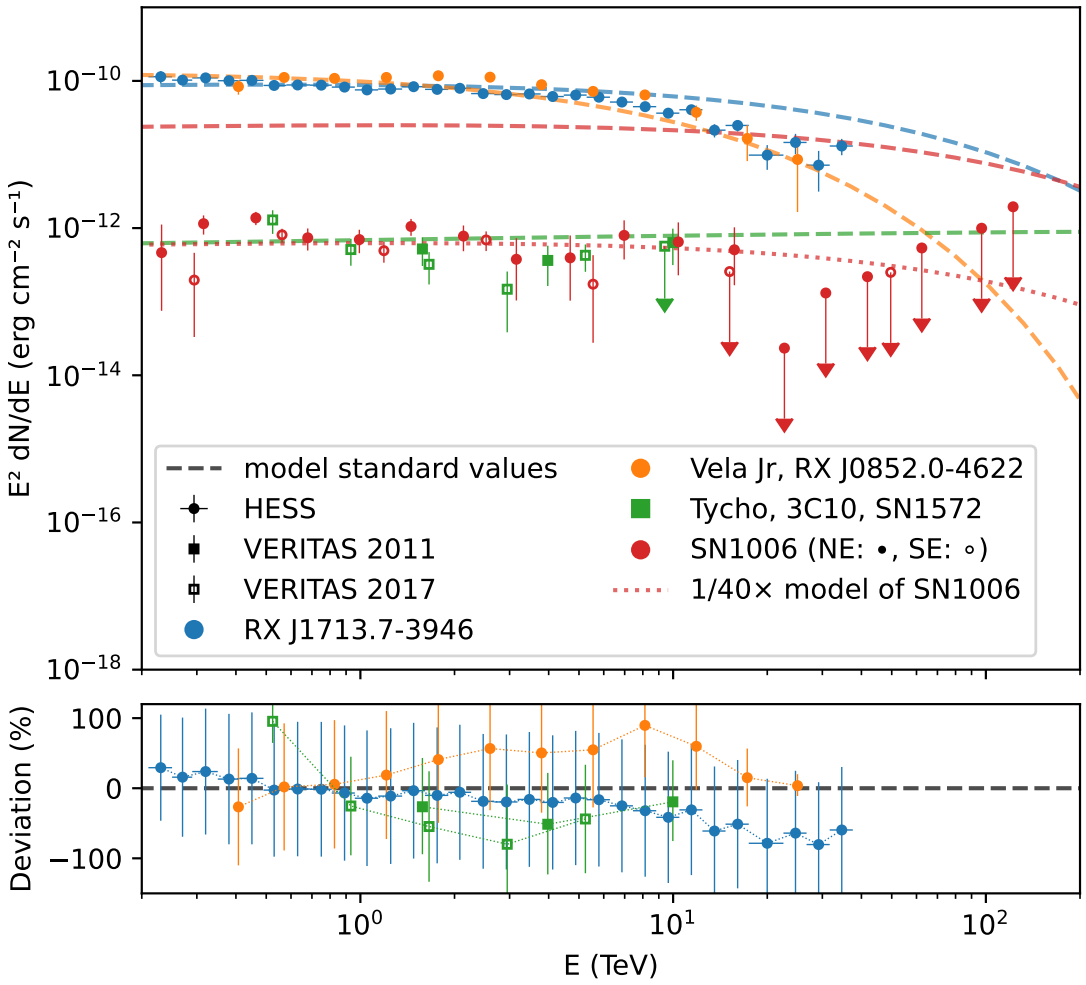

Figure 13: The first plot contains the comparison of the model using standard values: ($\rho_0 = 1\,m_\mathrm{p}\mathrm{cm}^{-3}$, $\delta = 2.5$, $M_\mathrm{ej} = 10 M_\odot$, $B = 3\,\mu\mathrm{G}$)
The second plot contains the percentage deviation of the data from the model

energy that is derived from equation 3 as well as the radius at Sedov time in equation 9. As a result, not just the cutoffs in figure 19 vary, but also the flux. Apparently the curve of Tycho does not change, since its age is certain.

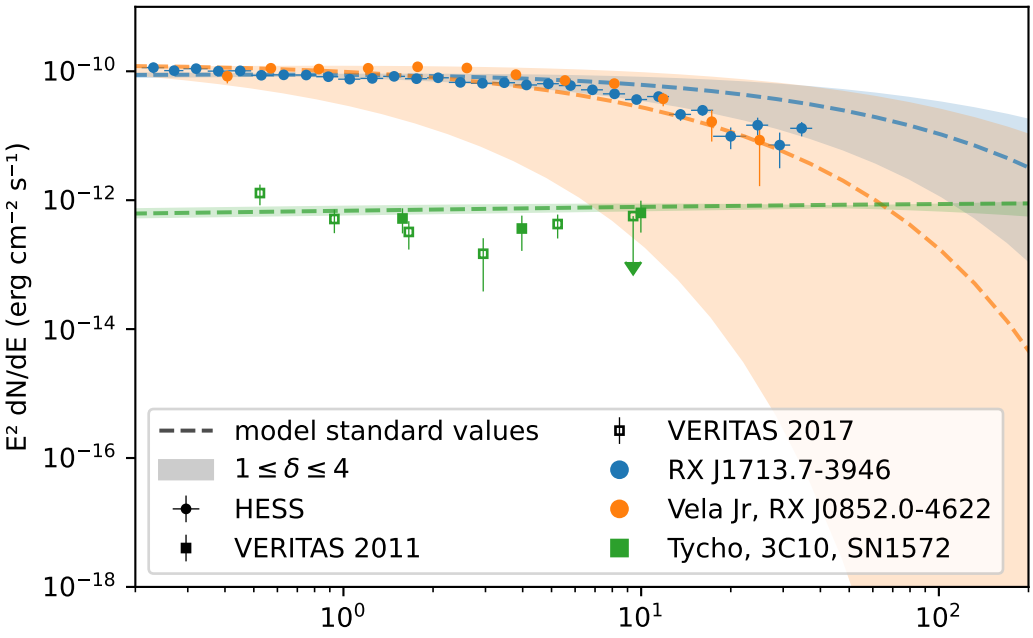

Figure 14: Varying the value of δ.

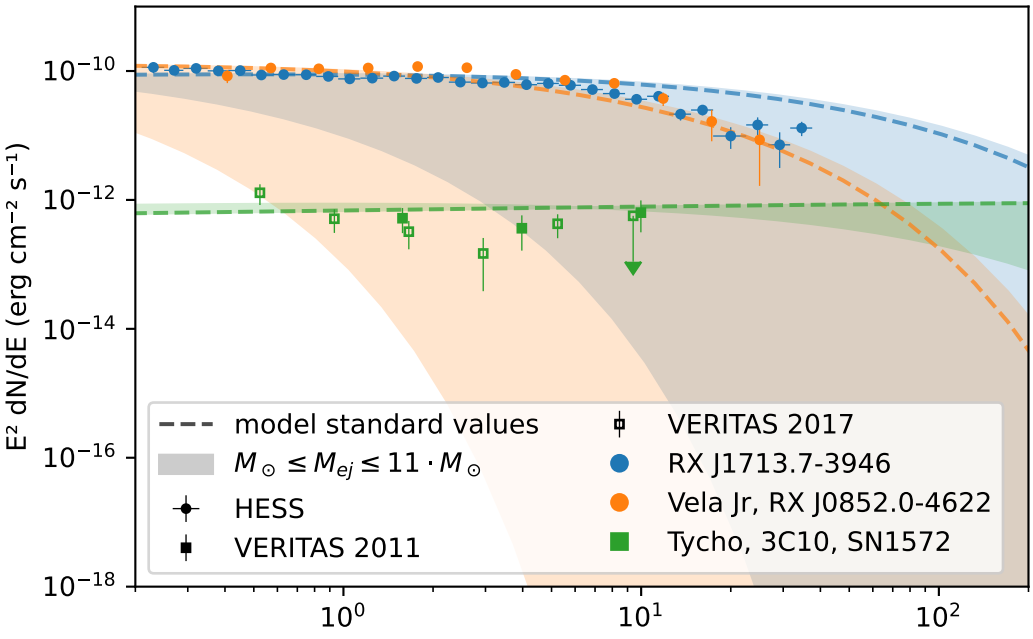

Figure 15: Varying the ejected mass

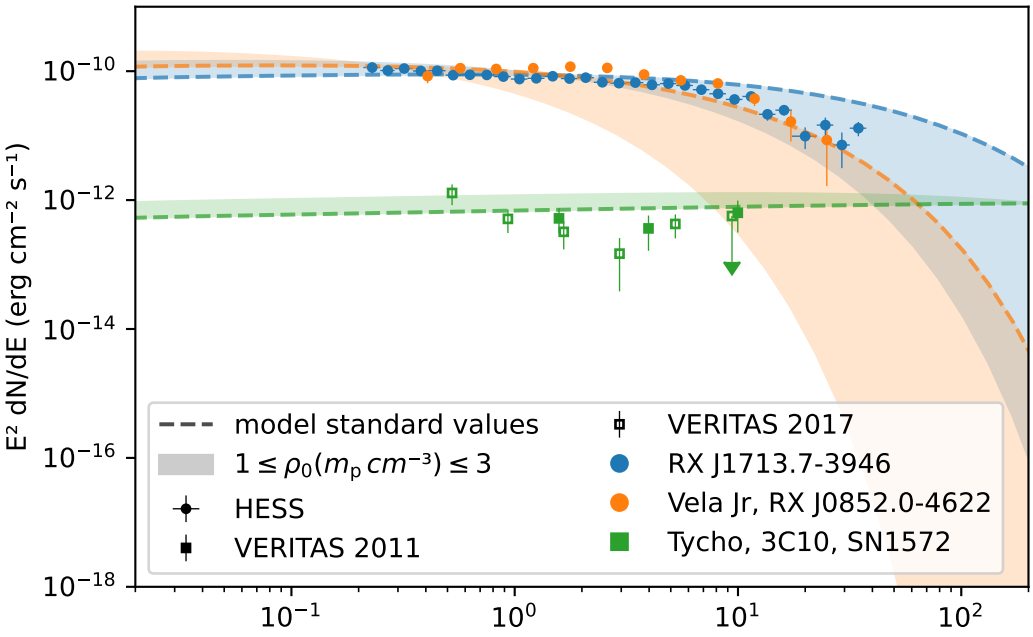

Figure 16: Varying the density of the ISM

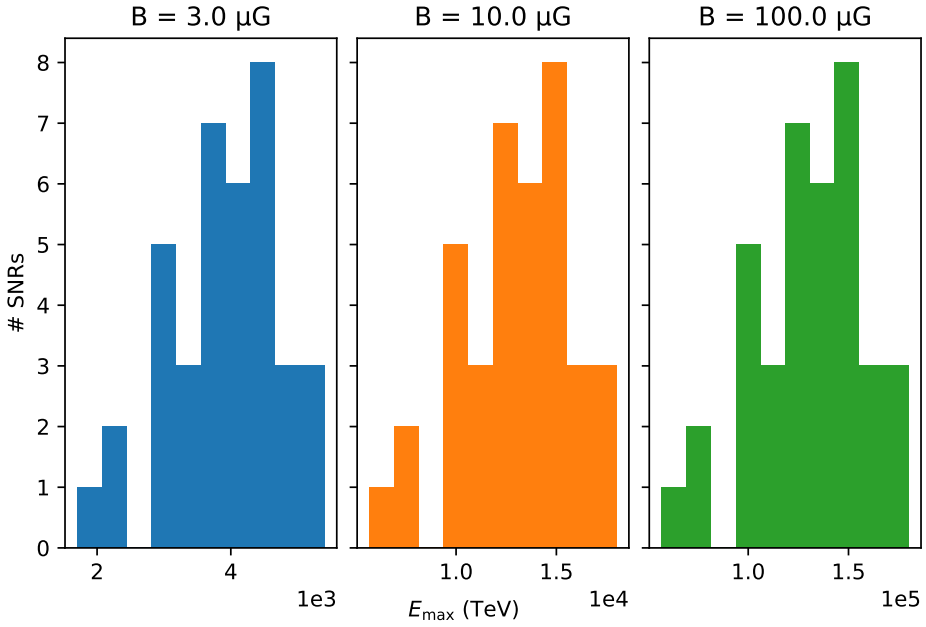

Figure 17: Histograms of the maximum energies under magnetic fields of different strengths

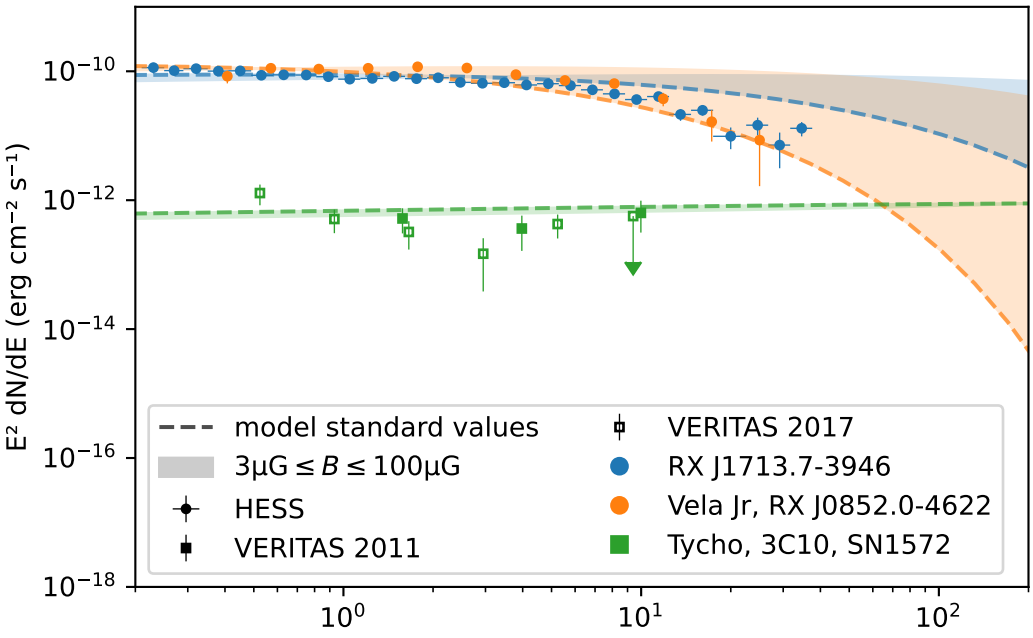

Figure 18: Varying the magnetic field

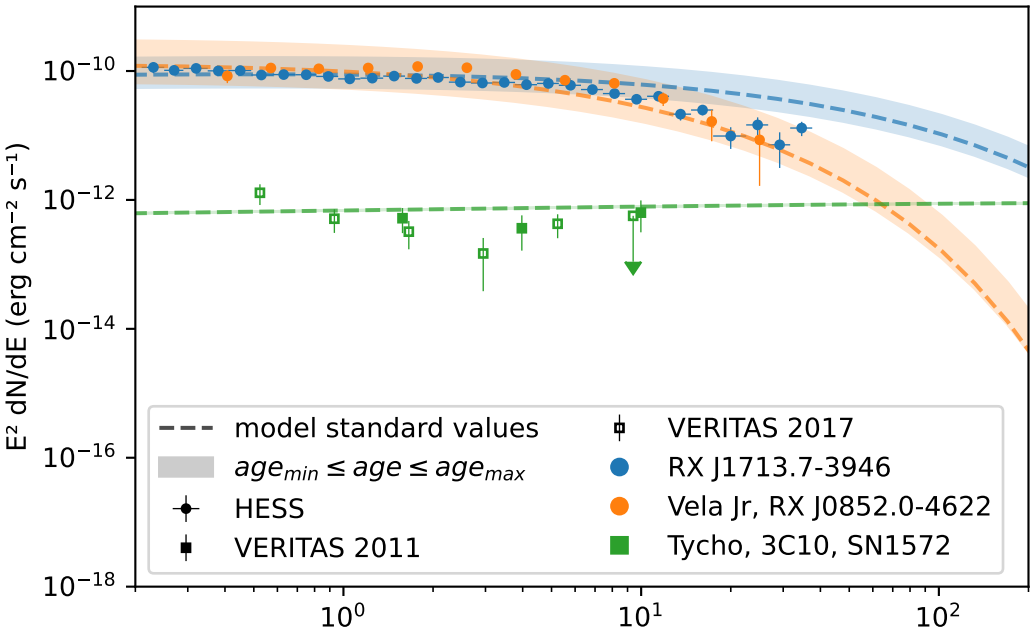

Figure 19: Taking the uncertainty on the SNRs age into account

To summarize it, the spectra that are calculated from the standard values do not exactly reflect the course of the data points, but slight changes that consider the individual conditions of each SNR can bring them closer. However, the influence this change has on the overall prediction of detectable SNRs can be neglected since the predicted SEDs are on the same order of magnitude as the data and thus are the fluxes.
It should also be noted that although the cutoff energy is definitely overestimated for a SNR that is younger than the predicted Sedov time, the predicted spectrum is comparable to the data, at least concerning the overall order of magnitude of the SED. Thus, the model and the resulting predictions are a good estimation of the group of SNRs that eventually will be detected by SWGO.
But besides its ability to give a reasonable prediction of detectable SNRs, the model has still limitations that need to be considered for more detailed studies on the detection of SNRs by SWGO.

4.2 Limitations of the Model

The model treats all SNRs as to be of similar kind, undergoing an equal evolution and expanding spherical into a homogeneus ISM. Thus it predicts a flux that is emitted isotropically from the SNR. However, this can result in too optimistic predictions as seen for SN1006, where there is only data for two spots of the SNRs whole extension. Also features like dust clouds that surround the SNR can have a strong influence on its evolution, e.g. Puppis A, where such clouds could have led to far less emission than expected. The proximity of other gamma-ray sources like in the case of Vela Junior can also be difficult since they might get indistinguishable for SWGO since it has a lower angular resolution according to detectors like HESS [5]. In relation to that, a SNR of a greater extent will be harder to detect since the detected gamma-rays are distributed over a greater angle. And since SWGO is a static detector, meaning it can't trace a source on the sky, some sources are longer visible due to their declination and the orientation of SWGO and therefor more data can be collected by SWGO than for other sources.
Another point is, that for the calculation of the gamma-ray spectra only p-p interactions were considered. Neglecting the contributions of the other production processes may not effect the prediction of detectable sources since p-p interactions are dominant over the other processes in the relevant energy regime. Nevertheless, the true spectrum and flux of each source is not represented. So the sources that clearly exceed the sensitivity curve of SWGO in figure 7 are most likely to be seen by SWGO. But those who only cross the sensitivity curve in a small region may not be definitely detectable because the measurable flux is quite low.
When the set of SNRs was selected, it was ensured that only confirmed SNRs were included. However, by detecting some of the sources of unclear origin, SWGO might help to determine their true nature and decide whether they are SNRs or not. That raises an interesting question: What can be expected and what can be learned from the potential detection of SNRs by SWGO?

5 Conclusion and Outlook

In this thesis a set of 38 SNRs was taken to predict the distribution of protons accelerated by them. With these particle spectra the individual gamma-ray spectra were predicted and compared to the sensitivity curves of SWGO. This allowed to decide for each SNR whether it will be detectable under given conditions or not. According to the model and the given standard values 8 SNRs were predicted to be detectable by SWGO.
To estimate how reasonable the predicted outcome is, the SEDs were compared to actual data. That showed that the predicted curves are close to the course of the data, but the cutoffs were overestimated. The deviations were attributed to the fact that the simplification of treating all SNRs equally neglects the individual conditions of each SNR. It was also shown that the model did not accurately apply to SNRs younger than the Sedov time due to the fact that the model uses equations that describe the SNR in the Sedov-Taylor phase.
But this mainly led to an overestimation of the cutoff energies, as the particle spectra and comparison showed. So the results were still trustworthy regarding the ability to detect these candidates with SWGO. However, for SNRs with fluxes close to the sensitivity curve the prediction of detectability by SWGO may be overestimated since the conditions that shift the SEDs have a stronger effect. The same applies to those SNRs were the measured date drastically differs from the expected curves like in the case of SN1006 or Puppis A.

By the detections of SWGO we will get a deeper insight into the SNRs in the southern sky. In this thesis, uncertain candidates were excluded to ensure that only SNRs were taken into account. However, SWGO might also help to determine whether some of these are SNRs or not. SWGO will also give new insights into the SNRs' structure and which mechanisms may influence its ability to accelerate particles. SWGO can also help to deeper understand the process of particle acceleration inside SNRs. And its sensibility to gamma-rays with energies up to a few hundred TeV can help to determine whether SNRs are PeVatrons or not and thus help to describe the origin of cosmic rays with energies beyond the knee in more detail. So with SWGO, we will get a better understanding of the nature of SNRs and their contribution to the local cosmic ray spectrum.

Source	Name	Detectable after 1 yr	Detectable after 5 yr	Detectable by HESS	Detected by HESS	Location	Flux for $E > 1$ TeV (TeV cm^{-2} s^{-1})	Flux for $E > 10$ TeV (TeV cm^{-2} s^{-1})
G347.3-00.5	RX J1713.7-3946	Yes	Yes	Yes	Yes	SH	1.67e-10	5.39e-11
G327.6+14.6	SN1006, PKS 1459-41	Yes	Yes	Yes	Yes	SH	6e-11	2.54e-11
G266.2-01.2	Vela Jr, RX J0852.0-4622	Yes	Yes	Yes	Yes	SH	1.04e-10	1.17e-11
G120.1+01.4	Tycho, 3C10, SN1572	Yes	Yes	Yes	No	NH	4.51e-12	3.44e-12
G260.4-03.4	Puppis A, MSH 08-44	Yes	Yes	Yes	(Yes)	SH	2.05e-11	1.6e-12
G309.2-00.6		Yes	Yes	Yes	No	SH	2.19e-12	8.89e-13
G315.4-02.3	RCW 86, MSH 14-63	Yes	Yes	Yes	Yes	SH	2.73e-12	6.95e-14
G089.0+04.7	HB21	Yes	Yes	Yes	No	NH	2.01e-12	8.49e-16
G111.7-02.1	Cassiopeia A (Cas A)	No	Yes	No	No	NH	1.16e-12	9.51e-13
G015.9+00.2		No	Yes	Yes	No	SH	7.59e-13	2.3e-13
G332.5-05.6		No	Yes	Yes	No	SH	1.2e-12	5.07e-14
G038.7-01.3		No	Yes	Yes	No	NH	6.93e-13	4.21e-14
G166.0+04.3	VRO 42.05.01	No	Yes	Yes	No	NH	5.86e-13	5.96e-15
G027.4+00.0	(Kes 73), 4C-04.71	No	No	No	(Yes)	SH	1.68e-13	1.2e-13
G033.6+00.1	Kes 79, 4C00.70, HC13	No	No	No	No	NH	1.98e-13	9.27e-14
G109.1-01.0	CTB 109	No	No	Yes	No	NH	6.11e-13	7.06e-14
G322.1+00.0	Circinus X-1	No	No	No	No	SH	1.51e-13	6.61e-14
G272.2-03.2		No	No	Yes	No	SH	4.27e-13	4.83e-14
G352.7-00.1		No	No	No	No	SH	9.73e-14	4.7e-14
G032.8-00.1	Kes 78	No	No	No	(Yes)	SH	1.51e-13	2.63e-14
G084.2-00.8		No	No	No	No	NH	3.07e-13	2e-14
G346.6-00.2		No	No	No	No	SH	5.3e-14	1.71e-14
G116.5+01.1		No	No	Yes	No	NH	3.68e-13	1.01e-14
G021.8-00.6	Kes 69	No	No	Yes	No	SH	3.91e-13	9.37e-15
G337.8-00.1	Kes 41	No	No	No	No	SH	6.89e-14	7.88e-15
G028.6-00.1		No	No	No	(Yes)	SH	5.8e-14	6.09e-15
G327.4+00.4	Kes 27	No	No	No	No	SH	2.1e-13	4.45e-15
G355.6-00.0		No	No	No	No	SH	2.59e-14	2.97e-15
G094.0+01.0	3C434.1	No	No	No	No	NH	9.46e-14	2.54e-15
G296.7-00.9		No	No	No	No	SH	1.08e-13	1.22e-15
G085.9-00.6		No	No	No	No	NH	5.55e-14	9.98e-16
G296.1-00.5		No	No	Yes	No	SH	1.91e-13	7.89e-16
G284.3-01.8	MSH 10-53	No	No	Yes	Yes	SH	2.61e-13	7.41e-16
G046.8-00.3	(HC30)	No	No	No	No	NH	1.16e-13	5.25e-16
G053.6-02.2	3C400.2, NRAO 611	No	No	No	No	NH	3.37e-14	6.44e-17
G357.7+00.3	the Square	No	No	Yes	No	SH	9.63e-14	8.53e-18
G359.1-00.5		No	No	No	(Yes)	SH	1.63e-14	2.36e-19
G082.2+05.3	W63	No	No	Yes	No	NH	7.46e-14	2.79e-20

Table 3: All 38 SNRs sorted by their detectability according to figure 7

References

[1] Acero, F. et al. "First detection of VHE s from SN 1006 by HESS". In: *A&A* 516 (2010), A62. DOI: 10.1051/0004-6361/200913916. URL: https://doi.org/10.1051/0004-6361/200913916.

[2] M. Ackermann et al. "The Search for Spatial Extension in High-latitude Sources Detected by the Fermi Large Area Telescope". In: 237.2, 32 (Aug. 2018), p. 32. DOI: 10.3847/1538-4365/aacdf7. arXiv: 1804.08035 [astro-ph.HE].

[3] Aharonian, F. et al. "A detailed spectral and morphological study of the gamma-ray supernova remnant RX J1713.7-3946 with HESS". In: *A&A* 449.1 (2006), pp. 223–242. DOI: 10.1051/0004-6361:20054279. URL: https://doi.org/10.1051/0004-6361:20054279.

[4] Aharonian, F. et al. "HESS very-high-energy gamma-ray sources without identified counterparts". In: *A&A* 477.1 (2008), pp. 353–363. DOI: 10.1051/0004-6361:20078516. URL: https://doi.org/10.1051/0004-6361:20078516.

[5] A. Albert et al. *Science Case for a Wide Field-of-View Very-High-Energy Gamma-Ray Observatory in the Southern Hemisphere*. 2019. DOI: 10.48550/ARXIV.1902.08429. URL: https://arxiv.org/abs/1902.08429.

[6] Silvia Celli. *Gamma-ray and Neutrino Signatures of Galactic Cosmic-ray Accelerators*. Cham, CH: Springer, 2019.

[7] Silvia Celli, Felix Aharonian, and Stefano Gabici. "Spectral Signatures of PeVatrons". In: *The Astrophysical Journal* 903.1 (Nov. 2020), p. 61. DOI: 10.3847/1538-4357/abb805. URL: https://doi.org/10.3847/1538-4357/abb805.

[8] Dubner, G. et al. "The most complete and detailed X-ray view of the SNR Puppis A". In: *A&A* 555 (2013), A9. DOI: 10.1051/0004-6361/201321401. URL: https://doi.org/10.1051/0004-6361/201321401.

[9] Yasuo Fukui et al. "Discovery of Interacting Molecular Gas toward the TeV Gamma-Ray Peak of the SNR G 347.3–0.5". In: *Publications of the Astronomical Society of Japan* 55.5 (Oct. 2003), pp. L61–L64. ISSN: 0004-6264. DOI: 10.1093/pasj/55.5.L61. eprint: https://academic.oup.com/pasj/article-pdf/55/5/L61/17448510/pasj55-0L61.pdf. URL: https://doi.org/10.1093/pasj/55.5.L61.

[10] H.E.S.S. Collaboration et al. "Deeper H.E.S.S. observations of Vela Junior (RX J0852.0-4622): Morphology studies and resolved spectroscopy". In: *A&A* 612 (2018), A7. DOI: 10.1051/0004-6361/201630002. URL: https://doi.org/10.1051/0004-6361/201630002.

[11] H.E.S.S. Collaboration et al. "H.E.S.S. reveals a lack of TeV emission from the supernova remnant Puppis A". In: *Astronomy &amp Astrophysics* 575 (Feb. 2015), A81. DOI: 10.1051/0004-6361/201424805. URL: https://doi.org/10.1051%2F0004-6361%2F201424805.

[12] Victor F. Hess. "Über Beobachtungen der durchdringenden Strahlung bei sieben Freiballonfahrten". In: *Phys. Z.* 13 (1912), pp. 1084–1091.

[13] Franz Linke. "Luftelektrische Messungen bei zwölf Ballonfahrten". In: *Abhandlungen d. Königl. Ges. d. Wissensch. zu Göttingen* 1.3 (1904). URL: https://gdz.sub.uni-goettingen.de/id/PPN251726223_0003.

[14] Cara E. Rakowski, John P. Hughes, and Patrick Slane. "Two New Ejecta-dominated Galactic Supernova Remnants: G337.2-0.7 and G309.2-0.6". In: *The Astrophysical Journal* 548.1 (Feb. 2001), pp. 258–268. DOI: 10.1086/318680. URL: https://doi.org/10.1086/318680.

[15] Stephen P. Reynolds. "Supernova Remnants at High Energy". In: *Annual Review of Astronomy and Astrophysics* 46.1 (2008), pp. 89–126. DOI: 10.1146/annurev.astro.46.060407.145237. eprint: https://doi.org/10.1146/annurev.astro.46.060407.145237. URL: https://doi.org/10.1146/annurev.astro.46.060407.145237.

[16] *Southern Wide-field Gamma-ray Observatory - Official Website*. URL: https://www.swgo.org/SWGOWiki/doku.php.

[17] Todor Stanev. *High Energy Cosmic Rays*. Cham, CH: Springer, 2021.

[18] A. E. Suárez et al. "An X-ray characterization of the central region of the supernova remnant G332.5-5.6". In: 583, A84 (Nov. 2015), A84. DOI: 10.1051/0004-6361/201526699. arXiv: 1510.01215 [astro-ph.HE].

[19] Elisa Resconi Thomas K. Gaisser Ralph Engel. *Cosmic Rays and Particle Physics*. Cambridge: Cambridge University Press, 2016.

[20] J. Kelly Truelove and Christopher F. McKee. "Evolution of Nonradiative Supernova Remnants". In: *The Astrophysical Journal Supplement Series* 120.2 (Feb. 1999), pp. 299–326. DOI: 10.1086/313176. URL: https://doi.org/10.1086/313176.

[21] Jacco Vink. *Physics and Evolution of Supernova Remnants*. Cham, CH: Springer, 2020.

Eidesstattliche Erklärung

Hiermit erkläre ich, dass ich die vorliegende Arbeit selbstständig und ohne fremde Hilfe verfasst und keine anderen Hilfsmittel als die angegebenen verwendet habe. Insbesondere versichere ich, dass ich alle wörtlichen und sinngemäßen Übernahmen aus anderen Werken als solche kenntlich gemacht habe.

Ort, Datum	Nick Scharrer